Royal Netherlands
Meteorological Institute
Ministry of Infrastructure
and Water Management

Wind turbine parametrisation in HARMONIE-AROME

B.J.H. van Stratum, S. Basu, I.L. Wijnant, J. Barkmeijer, J. Onvlee
and A.P. Siebesma

De Bilt, 2019 | Technical report; TR-377

Koninklijk Nederlands
Meteorologisch Instituut
Ministerie van Infrastructuur en Waterstaat

Wind turbine parameterisation in HARMONIE-AROME

Bart van Stratum[*†], *Sukanta Basu*[#], *Ine Wijnant*[*],
Jan Barkmeijer[*], *Jeanette Onvlee*[*], *Pier Siebesma*[#*]

[*]Royal Netherlands Meteorological Institute (KNMI)
[#]Delft University of Technology

[†]bart@vanstratum.com

Dutch *Offshore* *Wind* Atlas

Technical report; TR-377

December 6, 2019

Contents

1 | Introduction

Offshore wind power production in the European Union (EU) and specifically the North-Sea region is steadily increasing: the Dutch offshore capacity is expected to grow from ±1 GW in 2019 to ±11.5 GW in 2030, as part of a total expected increase to ±70 GW in the entire EU (WindEurope, 2017). Wind turbines produce electric energy by extracting kinetic energy from the atmosphere, thereby decelerating (and agitating) the air. This typically results in a downstream decrease in wind speed and increase in turbulence (e.g. Baidya Roy & Traiteur, 2010; Fitch et al., 2012). As wind farms grow – both in size and number – the impact on weather and climate is expected to become more significant, requiring an adaptation of mesoscale models like HARMONIE-AROME (hereafter: HARMONIE) to account for the influence of wind farms on the local and regional meteorological conditions.

As part of the Dutch Offshore Wind Atlas (DOWA) project[1], we implemented the wind turbine parameterisation from Fitch et al. (2012) in HARMONIE. In the presence of wind turbines, this parameterisation adds an elevated drag term to the atmosphere, which locally decelerates the flow. The kinetic energy that is extracted from the atmosphere, but not converted into electric power, is used as a source term of turbulence kinetic energy (TKE).

As a first validation of the new wind turbine parameterisation in HARMONIE, four 48-hour experiments were compared to both experiments with the original code of Fitch et al. (2012) in WRF-ARW (hereafter: WRF), and available offshore measurements near the Dutch/Belgium coast.

Next, we repeated 6 months of the DOWA reanalysis with the wind farm parameterisation and all current offshore wind farms in the North-Sea region included. The motivation for this experiment was twofold: first, to more thoroughly validate the wind farm parameterisation. During the chosen period from January to (including) June 2016, two floating lidars were available in the Borssele wind farm zone, one

[1] www.dutchoffshorewindatlas.nl

in the Westermost Rough wind farm, with additionally FINO1 tower measurements near the Alpha Ventus wind farm. Since all these measurements are in or near existing wind farms, they are ideal for validating the new wind farm parameterisation. Secondly, the six month experiment allowed us to quantify the impact of the offshore wind farms on the Dutch offshore and coastal meteorological conditions.

The content of this report is as follows: chapter 2 describes the wind farm parameterisation in HARMONIE, including a description of the code organisation and required input files. Chapter 3 contains the brief validation of HARMONIE with WRF, followed by the description and analysis of the 6 month HARMONIE reanalysis in chapter 4. Finally, this report is concluded in chapter 5.

2 | Model description

2.1 | HARMONIE-AROME

The wind farm parameterisation is implemented in HARMONIE (cycle 40h1.2tg2), a mesoscale model developed by the ALADIN-HIRLAM consortium[1], which is operationally used in 10 European countries (Bengtsson et al., 2017). The base version contains several minor modifications, mostly related to the ERA5 boundaries and statistics output (Wijnant et al., 2019), and the data-assimilation (Fischer et al., 2005; Gustafsson et al., 2018) of Mode-S EHS aircraft (e.g. de Haan, 2011, 2016) and *Advanced Scatterometer*[2] (ASCAT) observations. Additional changes related to the wind farm parameterisation are described in the remainder of this chapter. See Chapter 6 for details on archiving and availability of the code.

2.2 | Wind farm parameterisation

This section briefly summarises the wind farm parameterisation from Fitch et al. (2012). For details, see the original publication.

The wind farm parameterisation of Fitch et al. (2012) imposes an elevated momentum sink on the mean flow, where the drag (or thrust) of the individual turbine blades is modelled as a constant (but wind speed dependent) drag force across the area swept by the rotor blades. As the diameter of a wind turbine is about an order of magnitude smaller than the horizontal grid spacing in HARMONIE (currently: 2.5 km), the model accounts for the bulk influence of one or several wind turbines per grid point.

The wind turbine characteristics are defined by the geometry (hub-height z_{hub} and turbine radius r), the cut-in (V_{in}) and cut-out (V_{out}) wind speeds, and by the

[1] www.hirlam.org
[2] http://projects.knmi.nl/scatterometer/ascat_osi_co_prod/

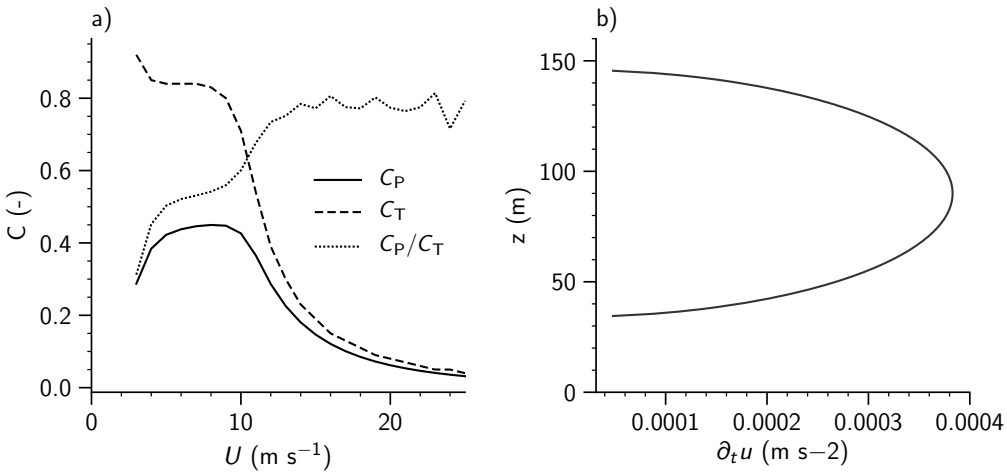

Figure 2.1: a) Example thrust and power coefficients, from a Vestas V112 turbine. For this model, $V_{in} = 3$ m s^{-1} and $V_{out} = 25$ m s^{-1}. b) Example of the momentum sink as a function of height, for a wind speed (constant with height) of 15 m s^{-1}, and a turbine with z_{hub}=90 m, r=56 m.

dimensionless power (C_P) and thrust (C_T) coefficients. The latter two describe – as a function of wind speed V_{hub} at hub height – the fraction of kinetic energy that is extracted from the air (C_T), and the fraction that is converted into electrical energy (C_P). An example of typical C_P and C_T curves is provided in Fig. 2.1a.

Given the thrust coefficient C_T, the thrust force of a turbine (the force opposite to the flow direction and drag force) is defined as:

$$\vec{F}_{\text{thrust}} = -\frac{1}{2}\rho C_T |\vec{V}|\vec{V} A_T, \qquad [\text{N}] \quad (2.1)$$

where ρ is the air density (kg m^{-3}), $\vec{V} = (u, v)$ the horizontal wind vector (m s^{-1}), $|\vec{V}| = \sqrt{u^2 + v^2}$, and A_T is the rotor area (m^2). The rate of loss of kinetic energy (KE) then equals:

$$\left.\frac{\partial \text{KE}}{\partial t}\right|_{\text{drag}} = -\frac{1}{2}\rho C_T |\vec{V}|^3 A_T. \qquad [\text{J s}^{-1}] \quad (2.2)$$

In practise, the rotor of a turbine intersects multiple model levels, and Eq 2.2 (and all equations in the remainder of this chapter) are solved for each model level k individually, replacing the rotor area A_T with the area intersected by the k-th grid level, and the wind speed $|\vec{V}|$, and density ρ with values from the k-th grid level, indicated where appropriate by a subscript k. As a result, the momentum sink (and

TKE source) is elevated and height dependent, as illustrated in Fig. 2.1b.

In general, the total change in KE of a single grid cell with a volume $\Delta_k = (\Delta x \Delta y \Delta z_k)$ m^3 equals:

$$\left.\frac{\partial \mathrm{KE_k}}{\partial t}\right|_{\mathrm{cell}} = \frac{\partial}{\partial t}\left(\frac{1}{2}\rho_k |\vec{V}_k|^2\right)\Delta_k = \rho_k |\vec{V}_k| \frac{\partial |\vec{V}_k|}{\partial t}\Delta_k. \quad [\mathrm{J\,s^{-1}}] \quad (2.3)$$

Combining Eqs 2.2 and 2.3, i.e. setting:

$$\left.\frac{\partial \mathrm{KE_k}}{\partial t}\right|_{\mathrm{cell}} = \left.\frac{\partial \mathrm{KE_k}}{\partial t}\right|_{\mathrm{drag}}, \quad [\mathrm{J\,s^{-1}}] \quad (2.4)$$

results, after re-arranging, in an expression for the change in velocity with time:

$$\frac{\partial |\vec{V}_k|}{\partial t} = -\frac{1}{2} C_{\mathrm{T}}\, |\vec{V}_k|^2\, A_k\, \Delta_k^{-1}, \quad [\mathrm{m\,s^{-2}}] \quad (2.5)$$

or, in component form:

$$\frac{\partial u_k}{\partial t} = -\frac{1}{2} C_{\mathrm{T}}\, u_k\, |\vec{V}_k|\, A_k\, \Delta_k^{-1}, \quad [\mathrm{m\,s^{-2}}] \quad (2.6)$$

$$\frac{\partial v_k}{\partial t} = -\frac{1}{2} C_{\mathrm{T}}\, v_k\, |\vec{V}_k|\, A_k\, \Delta_k^{-1}. \quad [\mathrm{m\,s^{-2}}] \quad (2.7)$$

The vertical velocity component is assumed to be unaffected by the wind turbines, and furthermore, drag by the wind turbine tower and nacelle is not included in the parameterisation. The energy that is extracted from the atmosphere, but not converted into electrical energy, is assumed to be converted into turbulence kinetic energy (TKE, per unit mass), i.e. $C_{\mathrm{TKE}} = C_{\mathrm{T}}$ - C_{P}, resulting in:

$$\frac{\partial \mathrm{TKE_k}}{\partial t} = \frac{1}{2} C_{\mathrm{TKE}}\, |\vec{V}_k|^3\, A_k\, \Delta_k^{-1}. \quad [\mathrm{m^2\,s^{-2}\,s^{-1}}] \quad (2.8)$$

Finally, as a diagnostic quantity, the model outputs the electrical power produced by the wind turbines:

$$\mathrm{P} = \frac{1}{2}\rho C_{\mathrm{P}}\, A_T\, |\vec{V}_{\mathrm{hub}}|^3 \quad [\mathrm{W}] \quad (2.9)$$

For a typical offshore wind farm, multiple wind turbines can occupy a single

horizontal grid point. Instead of introducing a horizontal wind turbine density – like in Fitch et al. (2012) – Eqs 2.6 to 2.9 are repeated for each individual turbine, allowing different turbine types in a single horizontal grid point.

2.3 | *Code description*

The majority of the wind farm parameterisation is implemented in a single Fortran module (`src/arpifs/module/windfarm_mod.F90`). This module contains two main subroutines, one which handles the initialisation (reading of turbine locations/types/properties, and mapping of the turbines to grid points), and one which calculates the tendencies of u, v and TKE each model time step using Eqs 2.6, 2.7 and 2.8, and the power production using Eq. 2.9. The wind farm parameterisation is called from `src/arpifs/phys_dmn/apl_arome.F90`.

2.4 | *Input files*

The wind farm parameterisation requires two sets of input files: one with the latitude, longitude and turbine type of each individual turbine (`wind_turbine_coordinates.tab`), and for each turbine type, a file with the turbine characteristics (`wind_turbine_xxx.tab`). The latter contains information on the turbine geometry, the thrust coefficients used below and above the cut-in and cut-out wind speeds, and a table with the power and thrust coefficients as a function of wind speed. The first and last wind speed included in the table defines the cut-in and cut-out wind speeds. Both file types are currently ASCII files, and need to be present in the `$HM_DATA/climate` directory before the start of the experiment.

Listing 2.1: Example input file of wind turbine locations
(`wind_turbine_coordinates.tab`*)*

```
#     lon         lat         type
    11.1640    56.6719         1
    11.1566    56.6543         1
    11.1903    56.6616         2
    11.1932    56.5400         2
    11.2373    56.5461         2
    -1.2358    56.5609         3
    -1.2185    56.6548         3
    -1.1886    56.5085         3
    11.1492    56.6689         4
```

Listing 2.2: Example input file of wind turbine characteristics
(`wind_turbine_004.tab`*)*

```
# Haliade-6 (z=100 m, D=150 m)
#    r (m)       z (m)     cT_low (-) cT_high (-)
    75.0000   100.0000      0.0500     0.0500
#   V (m/s)      cP (-)      cT (-)
     4.0000     0.3853      0.8600
     5.0000     0.4306      0.8600
     6.0000     0.4507      0.8600
# .......
    23.0000     0.0454      0.0600
    24.0000     0.0399      0.0500
    25.0000     0.0353      0.0500
```

3 | *WRF-HARMONIE intercomparison*

3.1 | Introduction

As a first validation of the new wind farm parameterisation in HARMONIE, we compared the results with data obtained from the original wind farm parameterisation in WRF. The comparison focussed on the Belgium *Northwind, C-Power, and Belwind* sites, located approximately 35 km of the Dutch/Belgium coast (Fig. 3.1). The comparison was mostly aimed at assessing whether the wind farm parameterisation in HARMONIE produces sensible results, i.e. whether HARMONIE produces a similar wake strength, increase in TKE, and power production. Where possible, the results were compared to measurements.

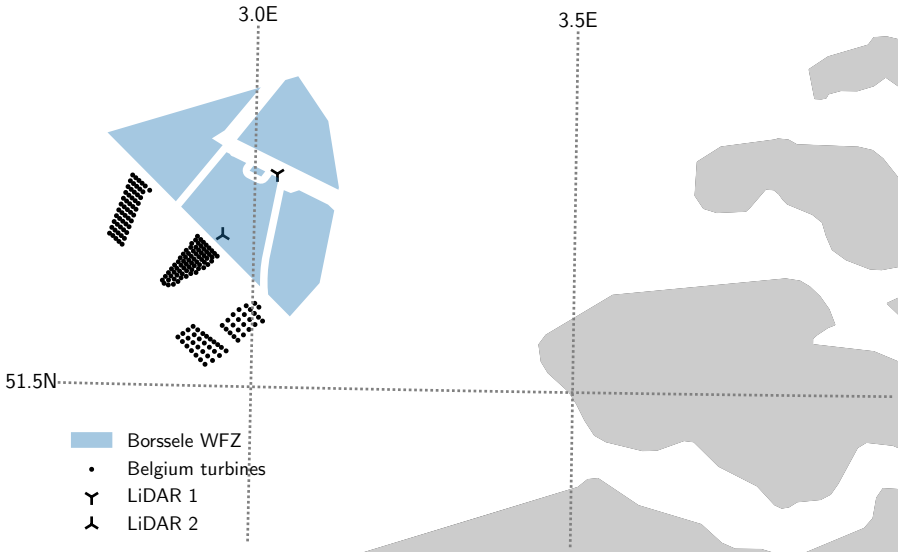

Figure 3.1: Existing Belgium wind turbines (individual dots), with the future Borssele wind farm zones.

3.2 | *Model setup*

HARMONIE (40h1.2tg2) used the same domain and experimental setup as used in the DOWA reanalysis (2000×2000 km^2 domain with 65 vertical grid levels, 2.5 km horizontal grid spacing, centred around 51.96°N, 4.9°E).

The WRF experiments were performed using the NOAH land surface model, MYNN2 boundary layer scheme, RRTMG long- and short wave radiation, and the single moment WSM 5-class microphysics scheme. The spatial grid was chosen to match the HARMONIE grid as closely as possible. However, a small spatial shift was still present, influencing the mapping of turbines to individual grid points, as shown in Fig. 3.2.

The wind turbine coordinates were obtained from Whiffle[1], the turbine characteristics from Delft University of Technology. The turbine locations and characteristics are archived as described in Chapter 6.

Both HARMONIE and WRF used ERA5 for the initial and boundary conditions, and performed 48 hour time integrations, for simplicity without data assimilation. Four periods were considered: 2016-02-01 00 UTC to 2016-02-03 00 UTC, with both HARMONIE and WRF experiment with and without the wind farm parameterisation, and 2016-08-05 00 UTC to 2016-08-07 00 UTC (stable conditions), 2016-07-07 00 UTC to 2016-07-09 00 UTC (neutral conditions) and 2016-09-30 00 UTC to 2016-10-02 00 UTC (unstable conditions) with only experiments using the wind farm parameterisation. The comparison here focusses mostly on the first time period, as without reference experiments without wind turbines, it is difficult to quantify the impact of the turbine parameterisation.

3.3 | *Results*

3.3.1 | *Atmospheric impact of wind turbines*

Fig. 3.3 (a,b) shows time series of the 100m wind speed and TKE, averaged over all grid points with one or more turbines (Fig. 3.2), for the 2016-02-01 00 UTC to 2016-02-03 00 UTC period. Over the first 24 hours, both the wind speed and TKE are comparable in HARMONIE and WRF, both for the experiments with (WF) and without (REF) the turbine parameterisation. Including the wind turbine parameterisation

[1] http://www.weatherfinecasting.com/

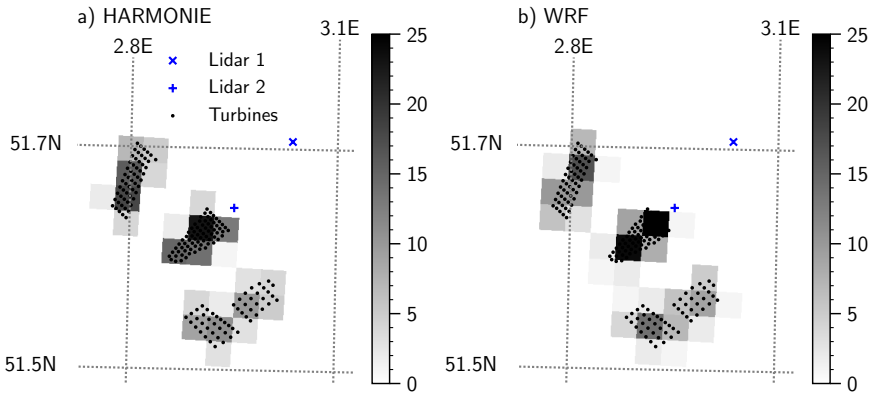

Figure 3.2: Mapping of wind turbines to grid points; the shading indicates the number of turbines per 2.5×2.5 km^2 grid point. Both lidars are part of the Borssele metocean campaign by Fugro

decreases the wind speed and increases TKE, as expected. Without data-assimilation or another mechanism to keep the models close to reality, the results start to drift apart over the second 24-hour period, hindering the comparison.

Fig. 3.3 (c,d) shows the same quantities, but as the difference between the experiments with and without the turbine parameterisation. The decrease in wind speed is similar in HARMONIE and WRF, but the increase in TKE is clearly higher in HARMONIE. This result can be explained by examining the time averaged vertical profiles, as shown in Fig. 3.4. The decrease in wind speed is comparable in both models, over the entire layer influenced by the wind turbines. However, the increase in TKE shows a different pattern; in HARMONIE the increase is mostly limited to the vertical extent of the wind turbines (∼0-200 m), whereas WRF mixes the increase in TKE over a deeper layer. Such differences outside the layer directly influenced by the turbine parameterisation are unlikely to be caused by the turbine parameterisation itself, and are more likely the result of differences in the vertical mixing schemes.

3.3.2 | *Power production*

Elia (Belgium's transmission system operator) provides time series of the observed total power production (P) of the offshore Belgium wind farms. As the power production scales with the velocity cubed (Eq. 2.9), it is very sensitive to errors in the modelled wind speed, and as such it is a useful parameter to both validate and compare HARMONIE and WRF.

Figure 3.5 shows the comparison between the Elia measurements, HARMONIE,

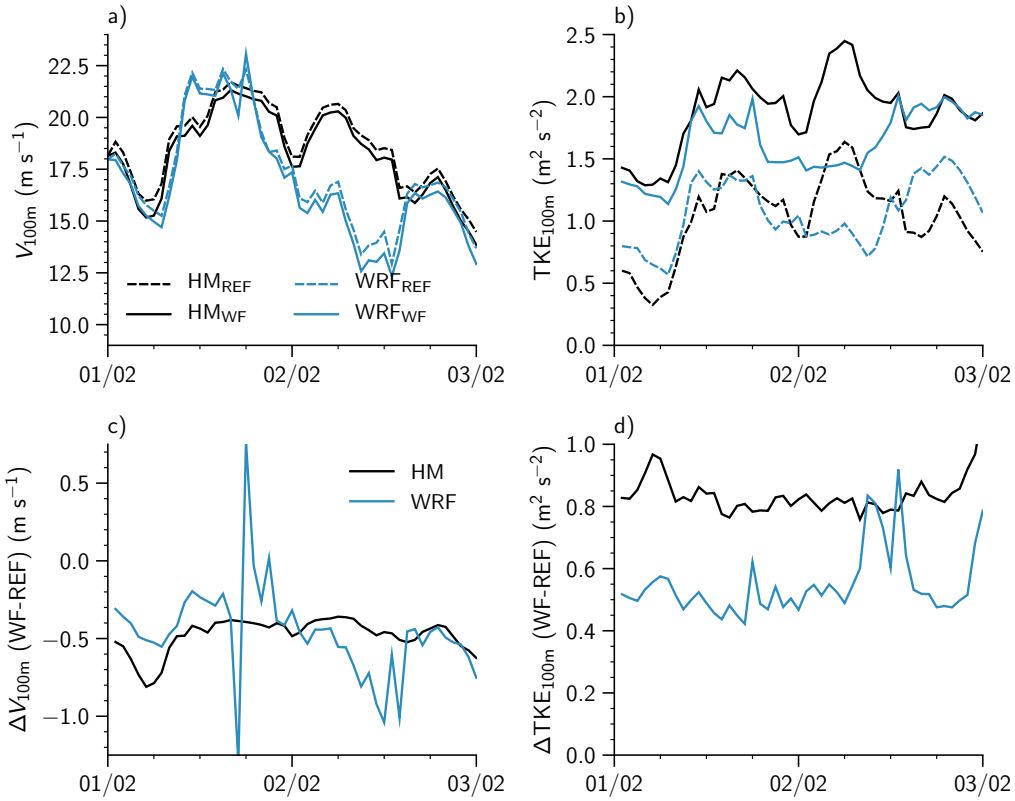

Figure 3.3: Top: time series of the 100 m wind speed and TKE from HARMONIE (HM) and WRF, with (WF) and without (REF) the wind turbine parameterisation. Bottom: differences between the WF and REF experiments, for both models.

and WRF. For all experiments the power production from the HARMONIE experiments without wind turbines is included as well, which was simply diagnosed offline from the model output using Eq. 2.9.

During the first time period (01-02-2016 to 03-02-2016), the wind speed was mostly such high that all three wind farms were operating at their peak (rated) power production. Theoretically, the three farms combined can produce ∼716 MW, which is reproduced by both HARMONIE and WRF. However, the measurements show a clear upper limit of only ∼650 MW. There are several possible explanations for this discrepancy – e.g. efficiency losses, curtailment, or turbines which were offline for maintenance – but the exact reason for these differences could not be ascertained.

For the other three periods, when the wind farms were not operating at their rated power, the agreement between measurements and the model predictions is better. On average, both HARMONIE and WRF with the wind turbine parameterisation reproduce the observed power production over the entire range from 0 to ∼600 MW,

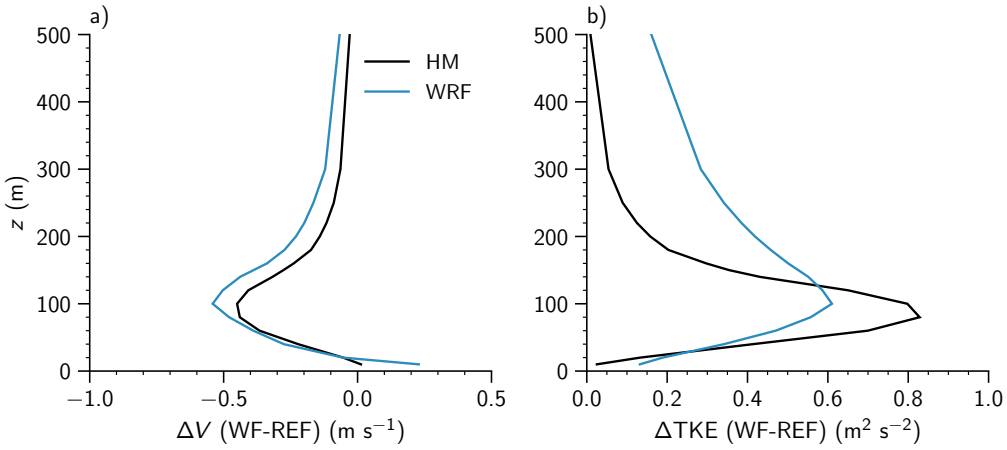

Figure 3.4: Time averaged vertical profiles of the difference in wind speed and TKE between the experiments with and without the turbine parameterisation.

without showing a clear bias. The power production diagnosed from the HARMONIE experiments without turbine parameterisation (HM_{REF}) shows a clear positive bias compared to the measurements. This indicated that the turbine parameterisation in both WRF and HARMONIE sufficiently reduces the wind speed to produce realistic power production estimates.

3.4 | *Conclusion*

The new wind turbine parameterisation in HARMONIE produces results which are comparable to results obtained from the original parameterisation in WRF. The local decrease in wind speed – caused by the wind turbine parameterisation – is nearly identical in both models, and the decrease in TKE is similar, although with a different distribution with height. Compared to the observed power production data from Elia, both HARMONIE and WRF perform similar. Furthermore, the predicted power production from HARMONIE with wind turbine parameterisation shows a clear improvement compared to the power production calculated from the experiments without wind turbines. Overall, these results gave confidence that the wind turbine parameterisation in HARMONIE is producing sensible results.

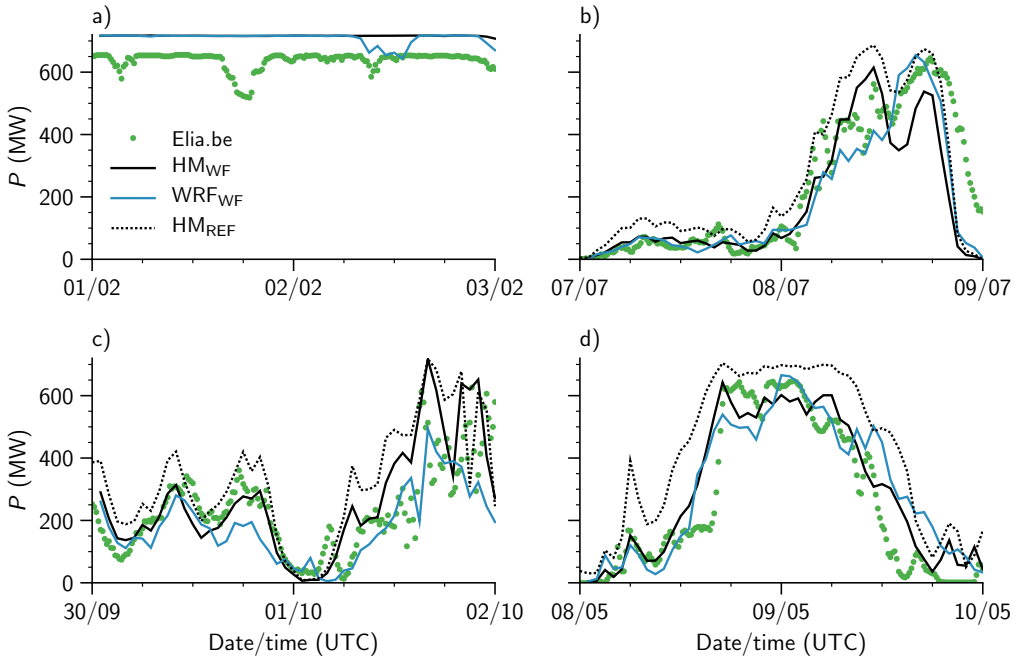

Figure 3.5: Power production compared to the measurements from Elia.be

4 | DOWA reanalysis with wind farms

4.1 | Introduction

To further validate the wind farm parameterisation with offshore measurements, and to quantify the impact of offshore wind farms on a typical HARMONIE experiment, we performed a 6 month reanalysis with all current offshore wind farms in the North-sea region included (Fig. 4.1).

The experiments were validated with wind speed measurements from two floating wind lidars in the Borssele wind farm zone (BWFZ), one platform mounted wind lidar at Westermost Rough wind farm and one mast mounted cup anemometer at FINO1. The experiments were also validated with power production data from the Belgium wind farms.

This chapter documents the experimental setup and provides a basic validation of the experiments, a more thorough validation is provided by Ramakrishnan (2019) as part of a MSc thesis at the Delft University of Technology.

4.2 | Wind turbine properties and locations

For the Belgium[1] and Dutch[2] wind farms, the exact (individual) turbine coordinates are available, which could directly be used in the experiments. For the other offshore wind farms in the computational domain (Fig. 4.1), the available information was limited to the wind farm boundaries and the total number of turbines per wind farm. For these sites, the turbine coordinates were first chosen randomly within the wind farm boundary, and next distributed uniformly using an iterative repulsion method (Witkin & Heckbert, 2005), as illustrated in Fig. 4.2. This random approach to determine the turbine coordinates can be justified by the fact that within the turbine

[1] Northwind, C-Power, and Belwind
[2] Egmond aan Zee, Princes Amalia, Luchterduinen, and Gemini

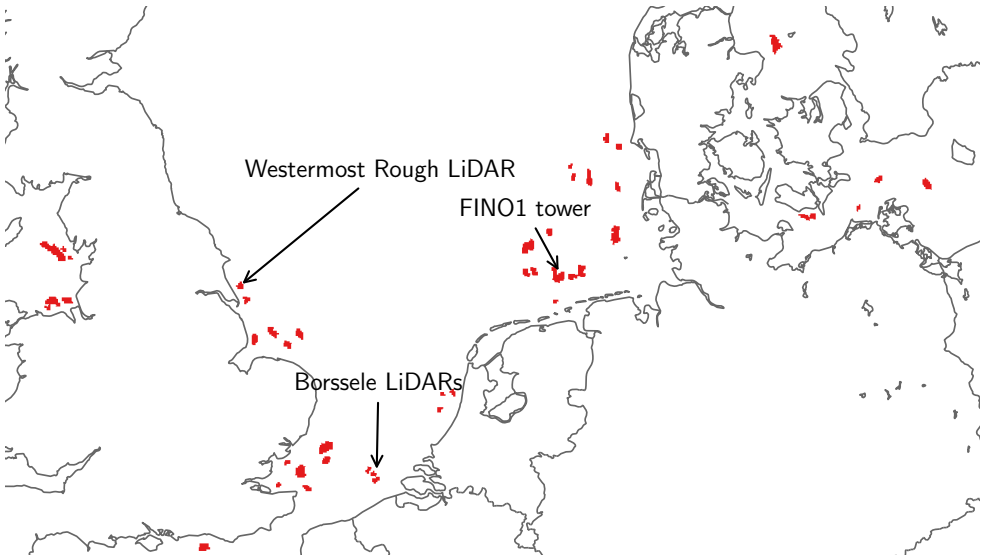

Figure 4.1: Overview of all (2.5×2.5 km) grid points with one or more wind turbines (red).

parameterisation, all turbines are mapped to the nearest 2.5×2.5 km grid point, making the exact turbine coordinates less important. The wind farm boundaries were obtained from the *The European Marine Observation and Data Network* (EMODnet)[3].

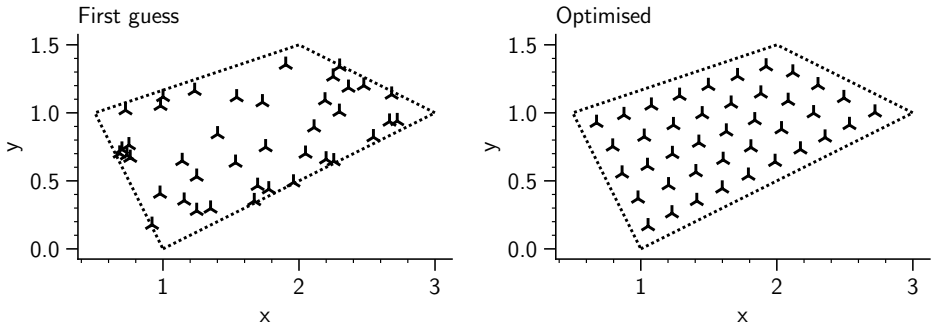

Figure 4.2: Example of the random placement of wind turbines within a known wind farm boundary, with (left) the first random guess, and (right) the final optimised locations.

The C_P and C_T curves were obtained from various sources, predominantly from windPRO[4]. For a small number of turbines, no C_P and C_T curves were publicly available, those turbines have been replaced with either reference data from literature, or

[3] https://www.emodnet-humanactivities.eu/search-results.php?dataname=Wind+Farms+(Polygons)
[4] https://www.emd.dk/windpro/

Name	N	P (MW)	D (m)	
Siemens SWT-2.3-82	72	2.3	72	
Siemens SWT-2.3-93	202	2.3	93	
Siemens SWT-3.6-107	563	3.6	107	
Siemens SWT-3.6-120	899	3.6	120	
Siemens SWT-4.0-120	78	4.0	120	
Siemens SWT-4.0-130	222	4.0	130	
Siemens SWT-6.0-154	478	6.0	154	(1)
Siemens SWT-7.0-154	47	7.0	154	(1)
Vestas V80-2.0	170	2.0	80	
Vestas V90-3.0	251	3.0	90	
Vestas V112-3.0	188	3.0	112	
Vestas V112-3.3	15	3.3	112	
Vestas V112-3.45	116	3.45	112	
Vestas V164-8.0	139	8.0	164	(2)
Senvion 5	30	5.0	126	
Senvion 6.2	156	6.2	126	
BARD-5.0	80	5.0	126	(3)
Adwen-5.0	202	5.0	116	(3)
Haliade-6	1	6.0	100	
	3908	460×10^3		

Table 4.1: Overview of the wind turbine types included in the experiments. The total installed power equals $\sum N \times P$. Notes: (1) replaced with 6 MW reference turbine from Bulder et al. (2016), (2) replaced with 8 MW reference turbine from Bulder et al. (2016), (3) replaced with Senvion 5 turbine.

C_P and C_T curves from similar turbines. An overview is provided in Table 4.1.

All data (turbine locations and properties) are archived as described in Chapter 6.

4.3 | *Experiments*

The HARMONIE setup is identical to the setup of the original DOWA reanalysis. The experiments run from 01-01-2016 00 UTC to 01-07-2016 00 UTC. This period was chosen because of the availability of two floating lidars in the Borssele wind farm zone[5], directly north-east of the (Belgium) Northwind wind farm (Fig. 3.2 & 4.1). In addition, for this period there are tower measurements from the FINO1 platform[6], and lidar measurements from the Westermost Rough wind farm[7].

[5] https://offshorewind.rvo.nl/studiesborssele
[6] https://www.fino1.de/en/
[7] https://orsted.com/en/Our-business/Offshore-wind/Wind-Data

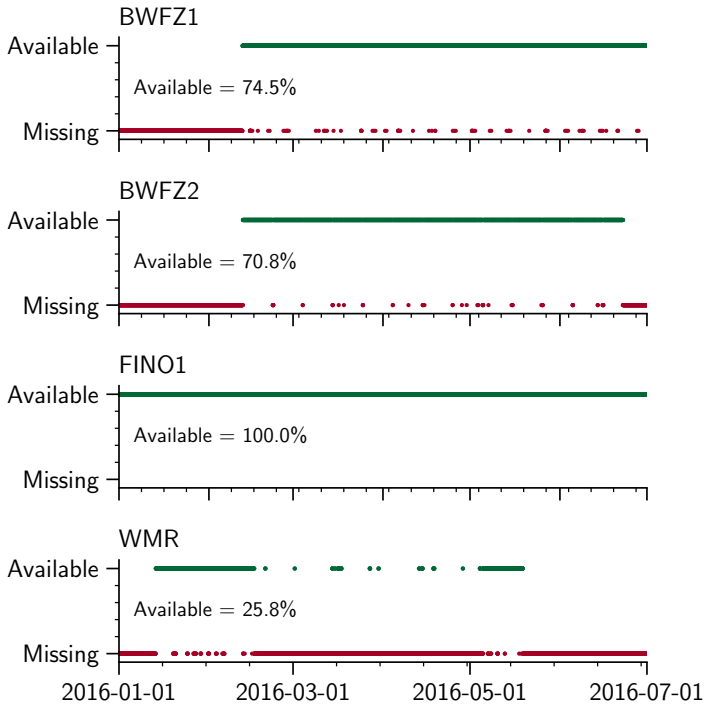

Figure 4.3: Availability measurements.

4.4 | *Validation*

The first part of the validation focusses on the offshore lidar and tower measurements. During the chosen period, all lidars had periods with missing data, as summarised in Fig. 4.3. The lidars in the Borssele wind farm zone (BWFZ) became operational in mid February, and have (overall) a good availability of measurements afterwards. The Westermost Rough (WMR) lidar became operational in mid January, but only has an overall availability of ∼25% (1.5 out of 6 months), which limits its usability.

For all statistical analyses in this chapter we use collocated data, i.e. missing data in the measurements is removed (or masked) in the model dataset as well. In addition, there is no conditional sampling based on (e.g.) wind direction; all available measurements are always included in the statistics.

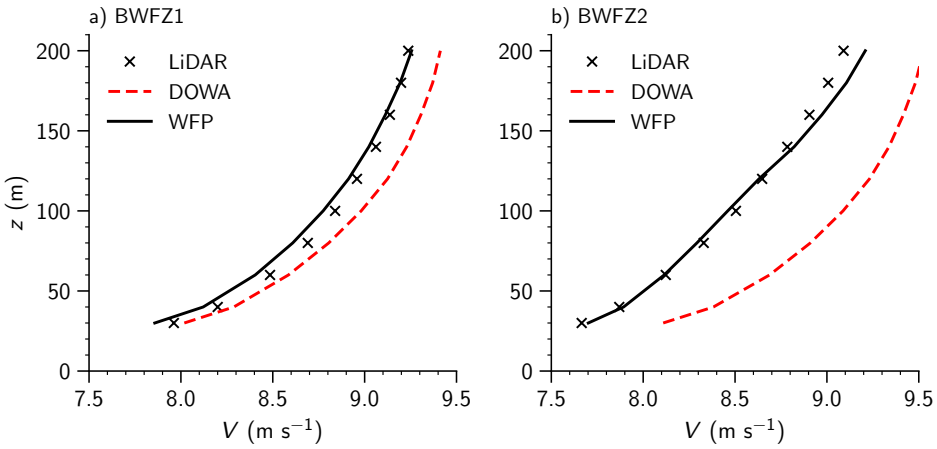

Figure 4.4: Vertical profiles of wind speed, from the normal DOWA reanalysis (DOWA) and experiment with wind farm parameterisation (WFP), compared to the Borssele lidars.

4.4.1 | Offshore lidar and tower measurements

Borssele Wind Farm Zone (BWFZ) lidars

As part of the wind resource assessment for the Borssele wind farm zone (BWFZ), Fugro[8] conducted a metocean campaign using (amongst other observations) two floating lidars. As shown in Fig. 3.1, both lidars were positioned north-east of the Belgium Northwind wind farm. With prevailing winds from the south-west, these lidar measurements are typically disturbed by the Belgium wind farms, making them ideal for assessing the impact of the wind turbines on the wind field, and the ability of the wind farm parametrisation to reproduce the disturbed wind field due to the wake effect of the wind farm.

Figure 4.4 shows the time averaged vertical wind speed profiles from the DOWA reanalysis (DOWA), the experiment with the wind farm parameterisation (WFP), and the Borssele lidars.

For both sites the DOWA reanalysis overestimates the wind speed, which is most pronounced for lidar location number two, which is closest to the Belgium wind farms. Enabling the wind farm parameterisation clearly improves the experiments; for location two, the mean profile from HARMONIE matches nearly perfect with the measurements, for location one the model slightly underestimates the wind speed.

[8] www.fugro.com

FINO1 tower

Approximately 50 km north of the Wadden island Borkum, the FINO1 research site provides continuous meteorological tower measurements at heights of 35 m to 100 m. The tower is situated directly west of the Alpha Ventus wind farm, and north-east of the Borkum Riffgrund wind farm (Fig. 4.1). Because of the measurement setup, with observations at only one side of the tower, the wind speed measurements need to be corrected to account for upwind blocking, lateral speedup, and downwind wake effects from the mast (Westerhellweg et al., 2012).

Fig. 4.5a shows the time averaged vertical wind speed profiles, compared to the corrected FINO1 measurements. In line with the results from the Borssele area, the DOWA reanalysis overestimates the wind speed with ∼0.6-0.8 m s^{-1}. With the wind farm parameterisation included, the absolute bias is decreased, but with a negative bias of ∼0.1-0.4 m s^{-1}. This underestimation seems to be partially caused by the mapping of wind turbines to the nearest HARMONIE grid point. In reality the FINO1 tower is west (and with the dominating wind direction: upstream) of the Alpha Ventus wind farm, but in HARMONIE the grid point nearest to FINO1 also houses some of the Alpha Ventus wind turbines, as shown in Fig. 4.5b. This means that the grid point used for the analysis, directly experiences drag from some of the Alpha Ventus turbines, resulting in a reduced wind speed.

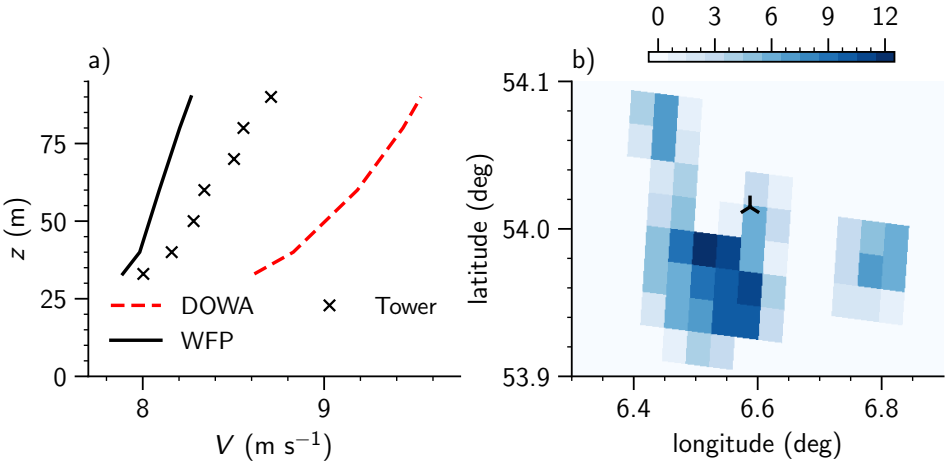

Figure 4.5: Vertical profiles of wind speed, from the normal DOWA reanalysis (DOWA) and experiment with wind farm parameterisation (WFP), compared to the FINO1 tower.

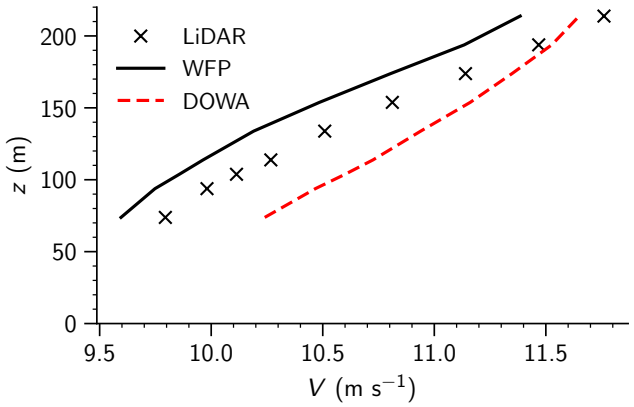

Figure 4.6: Vertical profiles of wind speed, from the normal DOWA reanalysis (DOWA) and experiment with wind farm parameterisation (WFP), compared to the Westermost rough lidar.

Westermost Rough lidar

On top of the Westermost Rough wind farm substation (Fig. 4.1), Ørsted operates a lidar, providing wind speed measurements between 74 m to 324 m height. Unlike the Borssele lidars and FINO1 tower, this lidar is located in the centre of the wind farm, and is therefore always disturbed by the wind turbines. As shown in Fig. 4.3, the data availability is limited to $\sim$ 25% of the January to June period, and even less at the three highest measurement heights. Therefore, the analysis here is limited to the lowest 214 m.

Fig. 4.6 shows the time averaged vertical profiles of the lidar measurements and HARMONIE experiments. As with the FINO1 location, the original DOWA reanalysis overestimates the wind speed, and the experiment with wind turbines has a smaller mean – but negative bias. However, overall the mean bias is relatively small at a maximum of -0.3 m s^{-1}.

4.4.2 | Power production

As mentioned in Chapter 3, power production is an interesting quantity to use for validation as it scales with the velocity cubed, making it sensitive to biases in wind speed. For the full period considered here, Elia provides power production data for the Belgium offshore wind farms.

Figure 4.7 shows the comparison between the observed power production and power production obtained from the HARMONIE experiments, both from the normal

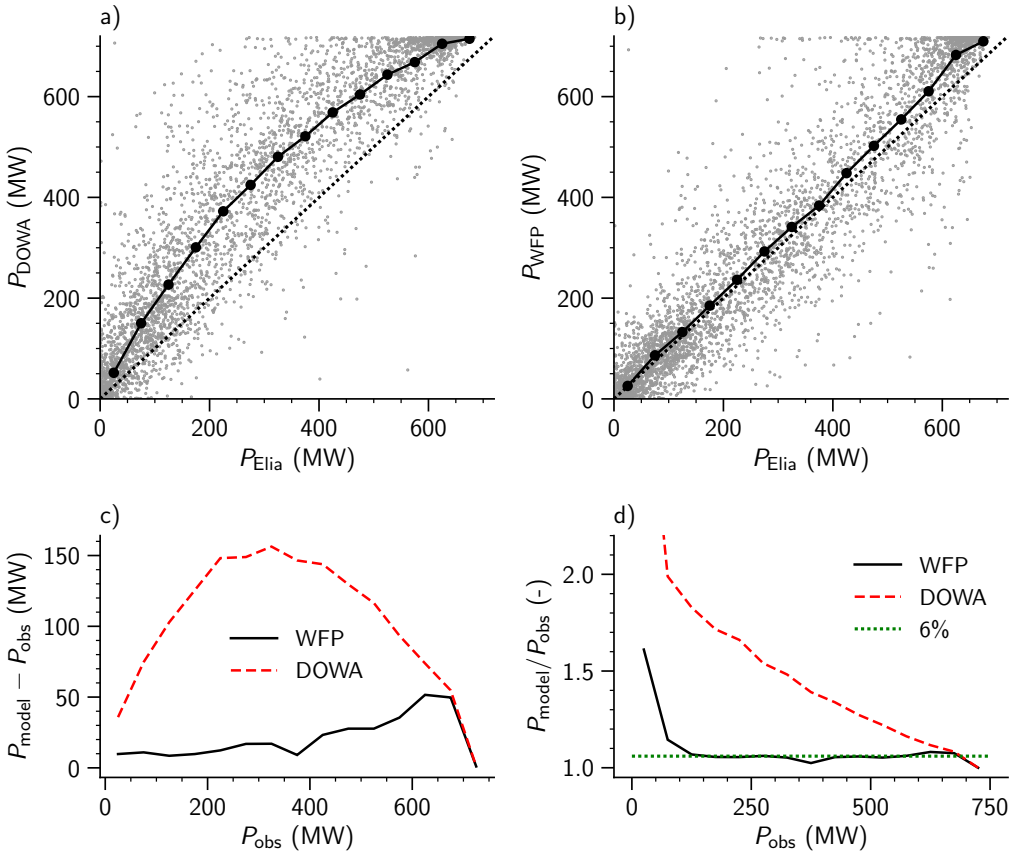

Figure 4.7: Power production calculated from the (a) normal DOWA reanalysis (REF) and (b) experiment with wind farm parameterisation (WFP), compared to the Elia measurements. The solid black line with markers (top row) indicates the mean of the model data calculated over 50 MW bins. The bottom row shows the absolute (c) and relative (d) error of both model experiments.

DOWA reanalysis (DOWA) and experiment with the wind turbine parameterisation (WFP). The bottom panels indicate the absolute and relative differences, averaged over 50 MW bins. The relative bias from the first (0-50 MW) bin should be treated with caution, as conditions where the observed power production equals zero result in an infinitely large relative bias.

The power production calculated offline from the DOWA reanalysis clearly overestimates the production, with absolute biases as large as 150 MW, and for low wind speeds (low power production) relative biases as large as 100%. Including the wind turbine parameterisation clearly improves the power production forecast, reducing the absolute bias to a maximum of 50 MW at high wind speeds, and the relative bias to ∼6%. There are a few possible causes for this constant relative bias – e.g. efficiency losses in the turbines or power cables, the use of (manufacturers) turbine specifications which are too optimistic, or inaccuracies in the turbine parameterisation – but the exact cause could not be traced.

4.4.3 | Impact wind farms on local meteorological conditions

As has become clear from the validation results, wind turbines have an impact on the (local) wind conditions. In addition, wind turbines generate TKE, which enhances vertical mixing, potentially influencing other quantities like temperature, humidity, or clouds.

In this section we briefly examine the impact of the Dutch offshore wind farms on the local meteorological conditions. In the absence of suitable measurements, the results are limited to comparing just the model results, from the original DOWA reanalysis and the experiments with wind turbines.

Fig. 4.8 shows the differences in wind speed (V), temperature (T), specific humidity (q) and relative humidity (RH) between the experiments with and without wind turbines. For each wind farm, the statistics were averaged over the HARMONIE grid points which have one or more turbines, and averaged in time.

For wind speed, the elevated drag is clearly visible, with a maximum decrease of -1 m s^{-1} near hub height, but a near-surface decrease which is almost zero. The relatively small wind farms near the Dutch west coast (*Egmond aan Zee*; 108 MW, *Princes Amalia*; 120 MW, *Luchterduinen*; 129 MW) have a smaller impact than the larger *Buitengaats* and *ZeeEnergie* (combined called *Gemini*; total of 600 MW) farms.

The enhanced vertical mixing has a weak impact on temperature and specific humidity. For these offshore locations, and for the period considered, the atmosphere is

on average stably stratified, with an increase in potential temperature and decrease in specific humidity with height. Additional vertical mixing tends to decrease the stratification, resulting in an increase in temperature and decrease in specific humidity near the surface, and decrease in temperature and increase in specific humidity at 100-150 m height. As a result of the near surface heating and drying, and the cooling and moistening aloft, the relative humidity decreases near the surface, and increases higher up. This could impact the formation of fog or low clouds, although no differences were visible in the cloud fraction output by the cloud scheme.

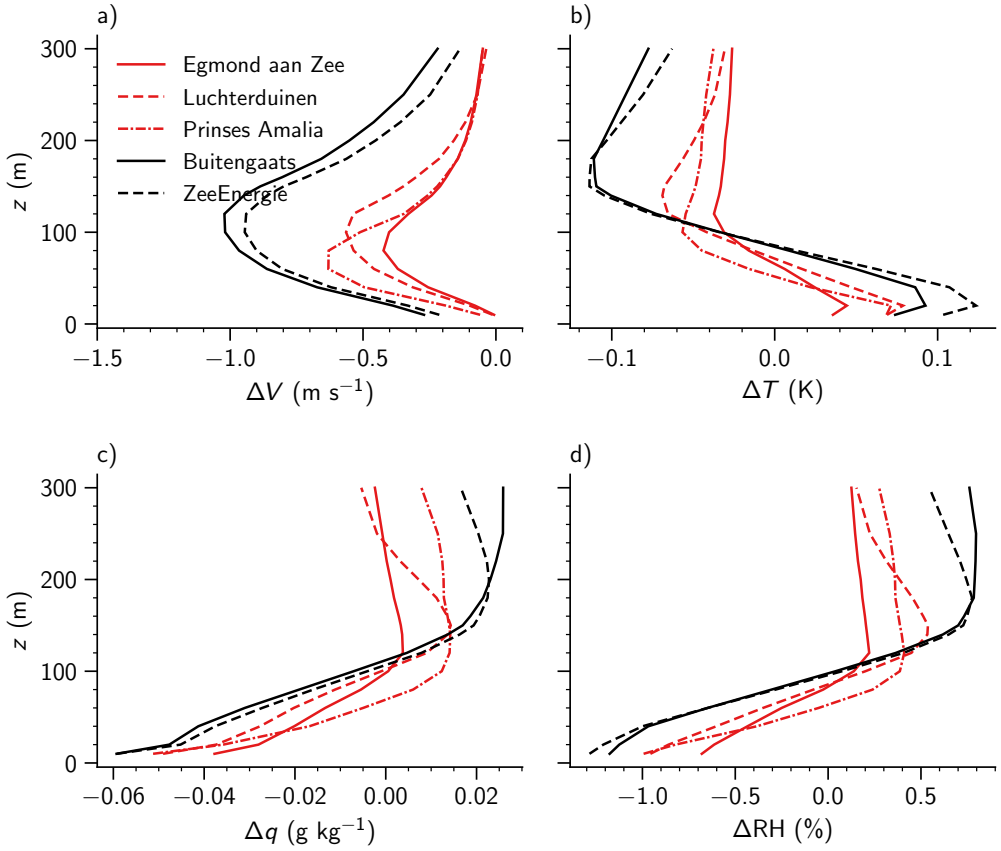

Figure 4.8: Impact wind turbines on meteorological conditions over the Dutch offshore wind farms.

4.5 | Conclusion

The validation of the six month reanalysis with wind turbines included, indicates that the inclusion of the turbine parameterisation has a positive impact on the predicted wind speeds near (offshore) wind farms. For all locations considered, the absolute

bias in wind speed is decreased compared to the original DOWA reanalysis. Furthermore, the predicted power production – compared to observations from Elia – shows a substantial improvement with the turbine parameterisation included.

A brief survey of the impact of wind farms on the local meteorological conditions, indicates that in addition to changes in wind speed, other quantities like temperature or humidity are influenced by wind farms as well.

5 | *Summary and conclusions*

This report described the efforts in the DOWA project to implement a wind turbine parameterisation in HARMONIE-AROME. In summary:

- The wind turbine parameterisation from Fitch et al. (2012) was successfully implemented in HARMONIE-AROME;
- Both the comparison with WRF, and the validation of the 6 month reanalysis with offshore measurements, indicate that the implementation is working in a physically meaningful way;
- The inclusion of the wind farm parameterisation improves the wind forecast near wind farms, where not accounting for the drag from wind turbines results in an overestimation of wind speed in HARMONIE-AROME.

The wind farm parameterisation is available to the HARMONIE-AROME community, with potentially interesting applications in both weather forecasting and research.

6 | *Code and data archiving*

The HARMONIE experiments are archived at ECMWF's tape archive (data, all paths starting with `ec:`) and the KNMI Gitlab account (code and scripts). All individual Gitlab directories have `README.md` files explaining the content of the directories.

Two different HARMONIE experiments were used:

- `DOWA_40h12tg2_fERA5_WF`: Initial *sanity check* against WRF and observations. The input files (turbine coordinates and properties) are stored inside the HARMONIE code directory:
  - HARMONIE code: https://gitlab.com/KNMI/RDWK/dowa/dowa_hm_home/tree/master/DOWA_40h12tg2_fERA5_WF
  - Output files: `ec:/nkbs/harmonie/DOWA/DOWA_40h12tg2_fERA5_WF/`
- `DOWA_40h12tg2_fERA5_WF2019_fix` (divided over `ptA` and `ptB`): Experiments with all 2016 wind farms. The input files are stored inside the HARMONIE code directory:
  - HARMONIE code: https://gitlab.com/KNMI/RDWK/dowa/dowa_hm_home/tree/master/DOWA_40h12tg2_fERA5_WF2019_fix
  - Output files:

    `ec:/nkbs/harmonie/DOWA/DOWA_40h12tg2_fERA5_WF2019_fix_ptA`

    `ec:/nkbs/harmonie/DOWA/DOWA_40h12tg2_fERA5_WF2019_fix_ptB`
  - Pre- and postprocessing scripts: https://gitlab.com/KNMI/RDWK/dowa/wind_farms_pre_post_proc.

References

Baidya Roy, S., & Traiteur, J. J. (2010). Impacts of wind farms on surface air temperatures. *Proceedings of the National Academy of Sciences*, *107*(42), 17899–17904.

Bengtsson, L., Andrae, U., Aspelien, T., Batrak, Y., Calvo, J., de Rooy, W., ... others (2017). The HARMONIE–AROME model configuration in the ALADIN–HIRLAM NWP system. *Monthly Weather Review*, *145*(5), 1919–1935.

Bulder, B., Bot, E., & Marina, A. (2016). *Scoping analysis of the potential yield of the Hollandse Kust (zuid) wind farm sites and the influence on the existing wind farms in the proximity* (Tech. Rep. No. ECN-E-16-021 - 2nd edt.) ECN.

de Haan, S. (2011). High-resolution wind and temperature observations from aircraft tracked by Mode-S air traffic control radar. *Journal of Geophysical Research: Atmospheres*, *116*(D10).

de Haan, S. (2016). Estimates of Mode-S EHS aircraft-derived wind observation errors using triple collocation. *Atmospheric Measurement Techniques*, *9*(8), 4141–4150.

Fischer, C., Montmerle, T., Berre, L., Auger, L., & Ştefănescu, S. E. (2005). An overview of the variational assimilation in the ALADIN/France numerical weather-prediction system. *Quarterly Journal of the Royal Meteorological Society*, *131*(613), 3477–3492.

Fitch, A. C., Olson, J. B., Lundquist, J. K., Dudhia, J., Gupta, A. K., Michalakes, J., & Barstad, I. (2012). Local and mesoscale impacts of wind farms as parameterized in a mesoscale NWP model. *Monthly Weather Review*, *140*(9), 3017–3038.

Gustafsson, N., Janjić, T., Schraff, C., Leuenberger, D., Weissmann, M., Reich, H., ... others (2018). Survey of data assimilation methods for convective-scale numerical weather prediction at operational centres. *Quarterly Journal of the Royal Meteorological Society*, *144*(713), 1218–1256.

Ramakrishnan, P. (2019). *Evaluation of a wind farm parameterisation in an operational mesoscale model* (Master's thesis, Delft University of Technology, the Netherlands). https://repository.tudelft.nl.

Westerhellweg, A., Neumann, T., & Riedel, V. (2012). "*FINO1 mast correction*" (Tech. Rep.). Retrieved from https://www.dewi.de/dewi/fileadmin/pdf/publications/Magazin_40/09.pdf

Wijnant, I. L., van Ulft, B., van Stratum, B. J. H., Barkmeijer, J., Onvlee, J., de Valk, S., C. Knoop, ... Klein Baltink, H. (2019). *The dutch offshore wind atlas (DOWA): description of the dataset* (Tech. Rep.). Retrieved from https://www.dutchoffshorewindatlas.nl/publications

WindEurope. (2017). *Wind energy in europe: Scenarios for 2030* (Tech. Rep.). Retrieved from https://windeurope.org/wp-content/uploads/files/about-wind/reports/Wind-energy-in-Europe-Scenarios-for-2030.pdf

Witkin, A. P., & Heckbert, P. S. (2005). Using particles to sample and control implicit surfaces. In *Acm siggraph 2005 courses* (p. 260).

Royal Netherlands Meteorological Institute

PO Box 201 | NL-3730 AE De Bilt
Netherlands | www.knmi.nl